

INJURY RISK ESTIMATION IN FAR-SIDE IMPACTS USING SMALL FEMALE AND AVERAGE MALE FINITE ELEMENT HUMAN BODY MODELS

Karan Devane

Bharath Koya

Ashley A. Weaver

F. Scott Gayzik

Biomedical Engineering,

Wake Forest University School of Medicine

USA

Fang-Chi Hsu

Department of Biostatistics and Data Science, Division of Public Health Sciences,

Wake Forest University School of Medicine

USA

Matthew Davis

Berkan Guleyupoglu

Elemance, LLC

USA

Paper Number 23-0149

ABSTRACT

Far-side crashes are the second-highest, after near-side impact crashes, cause of MAIS 3+ injuries to occupants for ΔV above 48 kph. The objective of this study was to estimate and compare injury risks between a small female and an average male occupant in far-side crashes using finite element human body models (HBM) in a simplified vehicle environment. To study far-side crashes, 126 simulations were conducted as a design of experiments (DOE) by varying lateral ΔV (10-50kph; 5kph increments), the principal direction of force (PDOF 50°, 60°, 65°, 70°, 75°, 80°, 90°), and occupant model. Occupant models used were the Global Human Body Models Consortium (GHBMC) 5th-percentile female (F05) and 50th-percentile male (M50) simplified models (-OS) with a modular detailed brain (+B). Overall skeletal structures are shared between the detailed and simplified models which allows the modular use of detailed parts in simplified models. Models were gravity settled and belted into a simplified vehicle model (SVM) modified for far-side impact simulations. The far-side SVM (FSVM) has both driver and passenger seats and door intrusion on the far side implemented. Acceleration pulses and vehicle intrusion profiles used for the DOE were generated by impacting a 2012 Camry vehicle model with a mobile deformable barrier model across the 7 PDOFs and 9 lateral ΔV 's in the DOE for a total of 63 additional simulations. The impacted surface of the Camry was instrumented to measure relative displacement into the vehicle to generate an intrusion profile. Injury risks were estimated for the head and chest (AIS2+; AIS3+) and abdomen and pelvis (AIS3+). Overall AIS3+ injury risk for each occupant was calculated using AIS3+ injury risk estimations for the head, chest, abdomen, and pelvis. A Wilcoxon signed-rank test was used to test for significant differences between estimated risks for F05-OS+B vs. M50-OS+B. Statistically significant differences between F05-OS+B and M50-OS+B were found for AIS2+ risk of head injury and AIS3+ risk of head, chest, and pelvis injury. No significant differences were found for AIS3+ risk of an abdominal injury and AIS2+ risk of chest injury. The overall risk of AIS3+ injury was higher for the M50-OS+B than the F05-OS+B in 84% of cases. Injury risk increased with an increase in lateral ΔV which was in agreement with studies found in the literature. An investigation of injury risks associated with far-side crashes was undertaken for both an average male and small female HBM. Differences observed in the estimated injury risks suggest that occupant size should be taken into consideration in safety system design. While this study used an FSVM with a rigid center console and dashboard, the relative differences between models were investigated. The effect of occupant size/sex on injury risk was highlighted by differences in overall injury risk for small female vs. average male HBMs. The study describes a method for simulating far-side crashes with an SVM that can include an estimation of intrusion.

INTRODUCTION

Even though 35% of side impact-related occupant injuries are due to far-side collisions [1] there are currently no regulatory tests for far-side scenarios in US-NCAP and the introduction of a far-side protocol in Euro-NCAP was in 2020 [2]. Analysis of real-world far-side crashes showed that the head and thorax are the two most frequently injured body regions followed by the abdomen [3]. The struck-side interior and the seatbelt are the first two contacting surfaces that cause injuries in far-side crashes [3, 4]. Currently, some vehicles may deploy all the side airbags so that a driver in a far-side crash could benefit from it but there are no countermeasures specifically designed to reduce injuries to far-side occupants. With the advancement in automotive technology, the far-side crash mode will become more relevant with highly automated vehicles (HAVs) with their non-standard seating configurations [5]. It is therefore necessary to develop different strategies to safeguard occupants in far-side crashes. Multiple studies have experimented with far-side events [6, 7], but their use for designing countermeasures is limited due to reduced boundary conditions. These studies did not take into account the effect of intrusion and/or deformable vehicle interiors. Experimental studies are expensive for performing parametric studies and it is not feasible to capture all the aspects of a real-world crash in laboratory tests.

On the other hand, computer simulations with finite element human body models (FEHBM) are one of the versatile tools for estimating injury risk in various scenarios as well as countermeasure development. Previous studies have demonstrated the use of FEHBMs for estimating injury risk in frontal, near-side, far-side, and rear impact events [2, 3, 5, 8-11]. Arun et al. studied occupant injuries and kinematics in far-side crashes using an occupant model in a full-scale vehicle model in 12 different scenarios [3], while Pipkorn et al. evaluated far-side airbags for reducing occupant injuries [2] by varying principal directions of force (PDOF). None of the studies so far has studied far-side crashes extensively using occupant models of different sizes and sexes, different PDOFs, and different impact velocities. All these variables affect injury risk to the occupant.

The objectives of this study were to estimate the injury risk in far-side impacts for small females and average males using FEHBMs, and then compare the results of the two models to check for differences in injury risk. The study used two FEHBMs representing small female and average male occupant models in a far-side simplified vehicle model (FSVM) in a parametric study by varying PDOF and lateral delta-V (ΔV).

METHODS

The Global Human Body Models Consortium small female (F05-OS+B v2.3) and average male (M50-OS+B v2.3) model with the detailed modular brain (from v6.0 detailed occupant models) were used in this study to simulate far-side crashes in an FSVM (Figure 1). A full-factorial design of experiment (DOE) was carried out using these two HBMs and varying lateral ΔV and PDOF. The lateral ΔV was varied in increments of 5 kph from 10 to 50 kph and seven different PDOFs (50°, 60°, 65°, 70°, 75°, 80°, and 90°) were used in the DOE. A total of 126 simulations were run as a part of the DOE. The acceleration pulses (longitudinal and lateral) and vehicle intrusion profiles for the DOE were generated by impacting a 2012 Toyota Camry model with a mobile deformable barrier (MDB) model at the 9 lateral ΔV and 7 PDOFs mentioned above to simulate a total of 63 far-side impact scenarios (Figure 2). The impacted surface of the Camry was instrumented to measure relative displacement into the vehicle to generate an intrusion profile, whereas vehicle acceleration pulses were measured using a seatbelt accelerometer attached to the floor at the bottom of the driver seat.



Figure 1. Far-side impact simulation setup with F05-OS+B model settled in a far-side simplified vehicle model

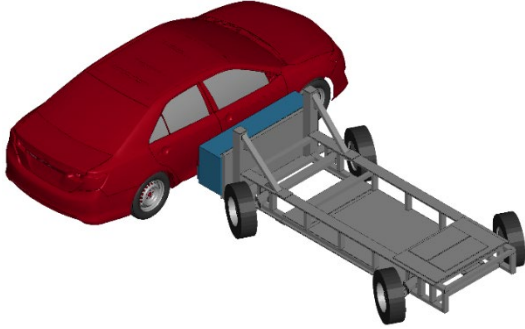


Figure 2. Toyota Camry-MDB far-side impact simulation setup

Each simulation with occupant models was run for 150 ms using LS-DYNA R10.2 (Ansys LSTC, Livermore, CA, USA). Both HBMs are instrumented to measure Head Injury Criterion (HIC), Brain Injury Criterion (BrIC), rib deflection, Combined Thoracic Index (CTI), abdominal force, and pubis force. All these injury metrics were used to estimate Abbreviated Injury Scale (AIS) 2+ and AIS3+ injury risk for the head and chest and AIS3+ injury risk for the abdomen and pelvis. The equations used for estimating all these injury risks were taken from previous studies (Table 1). Overall AIS3+ injury risk was calculated for each simulation using AIS3+ injury risk estimations for the head, chest, abdomen, and pelvis using the equation mentioned in Table 1. All the estimated injury risks for the M50-OS+B were compared to the F05-OS+B model injury risks. The matched-pair differences between the two models were checked for statistical significance using a Wilcoxon signed-rank test. R^2 was calculated to determine the proportion of variance of the estimate from one model that could be explained by the estimate from the other model using a linear regression model.

Table 1. Biomechanical risk curves used to determine model-based risk separated by body region, injury metric, and citation

Region	Metric	Equation	Citation
Head	HIC	$p(fracture) = \phi\left(\frac{\ln(HIC36) - \mu}{\sigma}\right)$ $AIS2+: \mu = 6.96352; \sigma = 0.84664$ $AIS3+: \mu = 7.45231; \sigma = 0.73998$	[12]
		$p(AIS2+) = \frac{1}{1 + e^{[(2.49 + \frac{200}{HIC}) - 0.00483 * HIC]}}$ $p(AIS3+) = \frac{1}{1 + e^{[(3.39 + \frac{200}{HIC}) - 0.00372 * HIC]}}$	[13, 14]
	BrIC	$p(AIS2+) = 1 - e^{-\left(\frac{BrIC}{0.602}\right)^{2.84}}$ $p(AIS3+) = 1 - e^{-\left(\frac{BrIC}{0.987}\right)^{2.84}}$	[15]
		$p(AIS2+) = 1 - \frac{1}{1 + e^{-(7.022 - (4.251 * BrIC))}}$ $p(AIS3+) = 1 - \frac{1}{1 + e^{-(8.549 - (4.251 * BrIC))}}$	[16]
Thorax	Rib Deflection	$p(AIS3+) = \frac{1}{1 + e^{(9.02937 - (0.03705 * (Age - 36.8232)) * Defl)}}$	[12]
	CTI	$p(AIS2+) = \frac{1}{1 + e^{(4.847 - (6036 * CTI))}}$	[17]
Abdomen	Abdominal Force	$p(AIS3+) = \frac{1}{1 + e^{6.04044 - (0.002133 * AbdForce)}}$	[12]
Pelvis	Pubis Force	$p(AIS3+) = \frac{1}{1 + e^{(9.7023 - (0.04678 * Age) - 0.0011 * Force)}}$	[12]
Overall	$P_{overall} = 1 - (1 - P_{head})(1 - P_{chest})(1 - P_{abdomen})(1 - P_{pelvis})$		

RESULTS

All 63 Camry-MDB and 126 simulations with two HBMs ran for 150 ms without any errors. The average solution times were 4 min/ms and 4.1 min/ms for M50-OS+B and F05-OS+B respectively. The results of the Wilcoxon signed-rank test and R^2 values of each injury risk comparison between the two models are reported in Table A1 in the appendix. The differences between the M50-OS+B vs. F05-OS+B model estimated injury risks were statistically significant ($p < 0.05$) except for the chest AIS2+ and abdomen AIS3+ injury risks. All the injury risks for the two models are cross-plotted in Figure 3 - Figure 9. All these figures include blue dots representing M50-OS+B injury risk on the x-axis and F05-OS+B model risk on the y-axis, a linear fit regression blue line for model risk points, and a black line of equivalence for reference. The closer all the dots are to the line of equivalence, the more similar the injury risk predicted by the two models. Also more points on the right of the line of equivalence the higher the M50-OS+B model estimated risk of injury and vice-versa. The M50-OS+B model estimated risks for all the body regions except the abdomen were higher than F05-OS+B. The overall injury risk was higher in 84% of cases for the M50-OS+B model. The BrIC-based head AIS2+ using Takhount et al. 2013 (Figure 5 left $R^2 = 0.95$) and chest AIS2+ (Figure 7 left $R^2 = 0.88$) injury risk were similar between the two models.

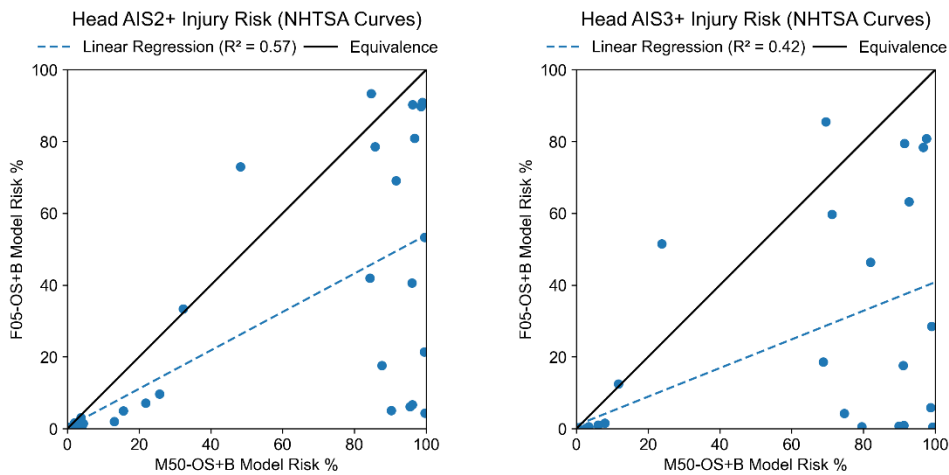


Figure 3. Cross-plot of the head injury risk (AIS2+: left, AIS3+: right) based on HIC using NHTSA curves [12]. M50-OS+B is on the x-axis and F05-OS+B is on the y-axis.

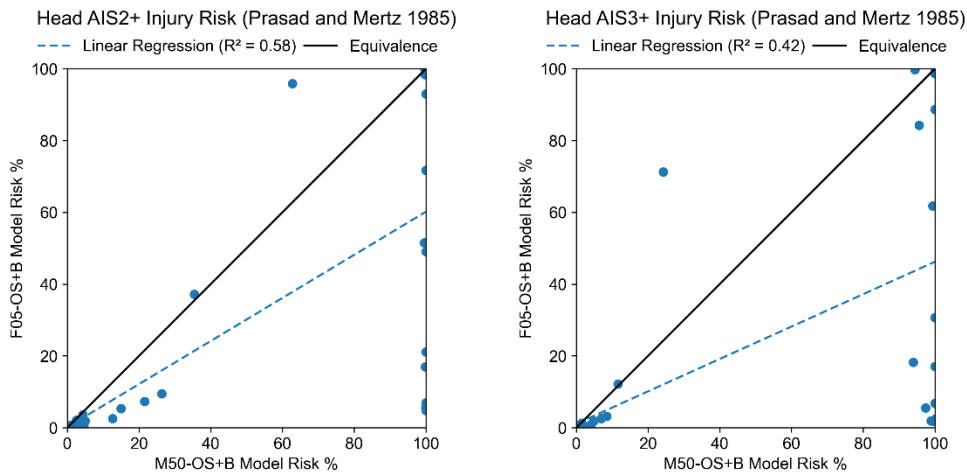


Figure 4. Cross-plot of the head injury risk (AIS2+: left, AIS3+: right) based on HIC using equations from Prasad and Mertz, 1985 [14]. M50-OS+B is on the x-axis and F05-OS+B is on the y-axis.

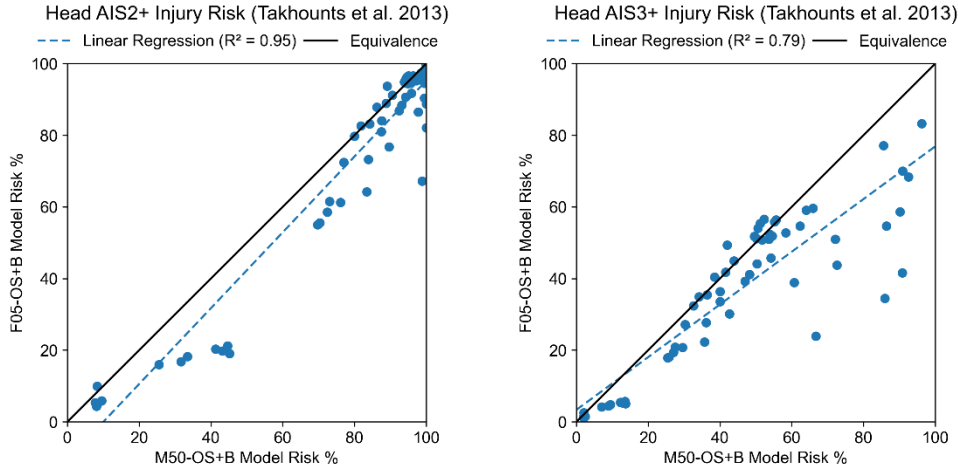


Figure 5. Cross-plot of the head injury risk (AIS2+: left, AIS3+: right) based on BrIC using equations from Takhounts et al. 2013 [15]. M50-OS+B is on the x-axis and F05-OS+B is on the y-axis.

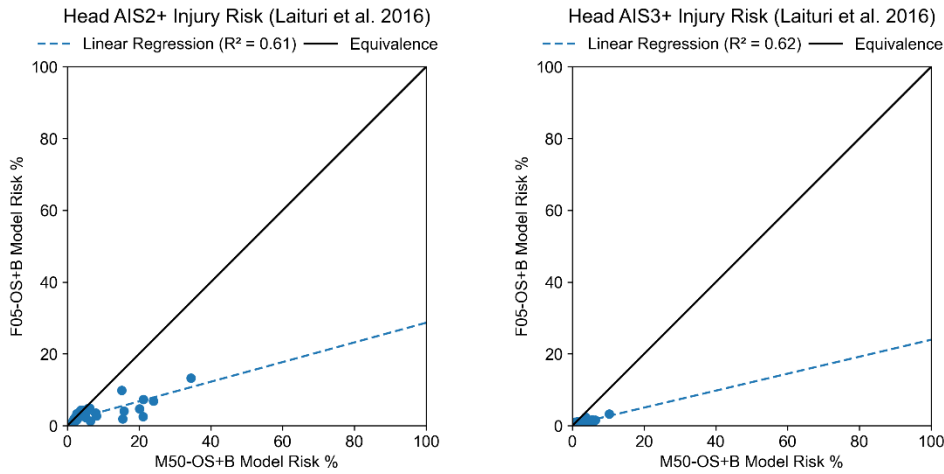


Figure 6. Cross-plot of the head injury risk (AIS2+: left, AIS3+: right) based on BrIC using equations from Laituri et al. 2016 [16]. M50-OS+B is on the x-axis and F05-OS+B is on the y-axis.

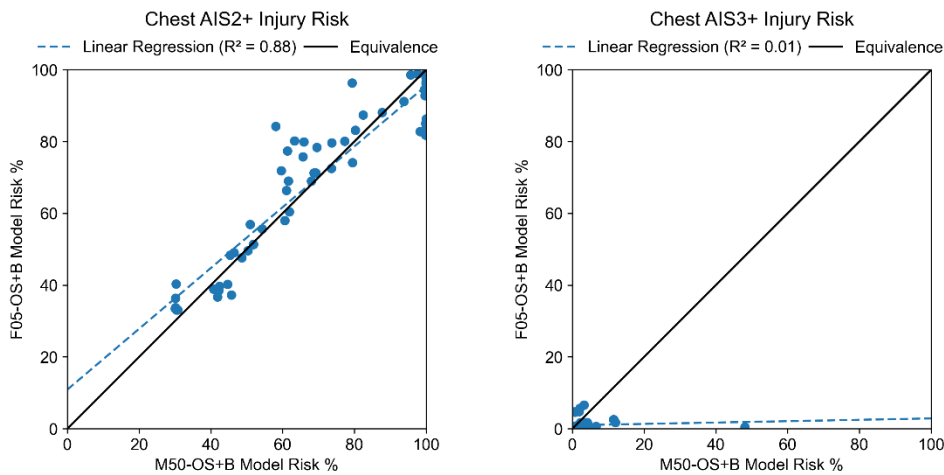


Figure 7. Cross-plot of the chest injury risk based on CTI (AIS2+: left) [17] and chest deflection (AIS3+: right) [12]. M50-OS+B is on the x-axis and F05-OS+B is on the y-axis.

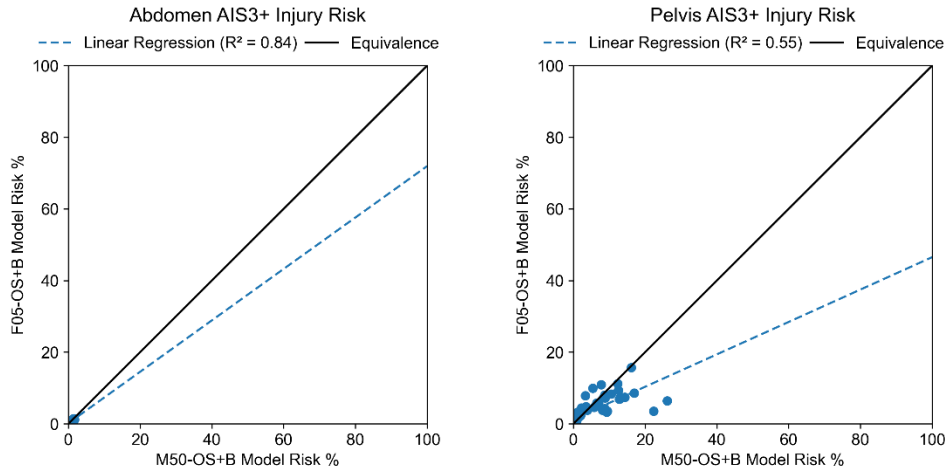


Figure 8. Cross-plot of the abdomen (left) and pelvis (right) AIS3+ injury risk based on abdomen and pubis force using equations from Kuppa, 2004 [12]. M50-OS+B is on the x-axis and F05-OS+B is on the y-axis.

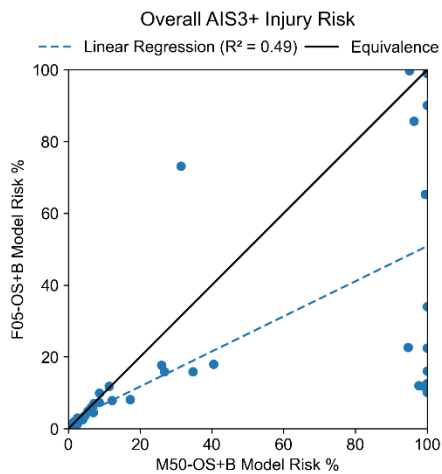


Figure 9. Cross-plot of the overall AIS3+ injury risk. M50-OS+B is on the x-axis and F05-OS+B is on the y-axis.

DISCUSSION

The objective of the current study was to simulate a variety of far-side impact scenarios using small female and average male occupant models and compare estimated injury risks. A total of 126 far-side crash simulations were simulated using two FEHBMs, 7 PDOFs, and 9 lateral ΔV s in an FSVM that included vehicle intrusion. Except for abdomen AIS3+ and chest AIS2+, the differences between all other injury risks were statistically significant ($p < 0.05$). The overall injury risk was higher in 84% of the cases for M50-OS+B than F05-OS+B suggesting the need for different countermeasures for different occupant sizes. A recent study by Klug et al. 2022 suggested that for robust assessment of vehicles in the virtual environment, a wide range of anthropometries should be considered. This study analyzed far-side crashes from multiple real-world crash databases from the US and Europe.

Due to the size differences between the two models the lateral motion was different. The male model had a higher lateral excursion in all the cases than the female model. Exemplar results of a far-side impact for ΔV of 50 kph at 90° PDOF at 5 different time points are depicted in Table A2 that shows higher lateral displacement for the male model. Both models contacted the far-side interior parts of the vehicle but the male model contacted more often than the female model. Shoulder seatbelt slippage may be one of the reasons for more lateral motion. With improved belt retention risk of injury will be lowered and this is one of the areas that need further investigation. The overall injury risk was increased with an increase in lateral ΔV but no trend was observed with a change in PDOF.

The study estimated AIS2+ and AIS3+ head injury risks using HIC and BrIC. In a previous study, AIS2+ head injury risk was estimated using the HIC-based Prasad and Mertz, 1985 [14] and BrIC-based Laituri et al. 2016 [16] equations which were better correlated with field-based injury risk data [18]. A similar study could be carried out in the future to compare all body region injury risks to real-world data using logistic regression equations from a literature study [19]. For both the models, head and chest injury risk were higher than injury risk for other body regions which was in line with what was reported by Digges and Dalmotas by analyzing real-world far-side crashes [4]. Although head and chest injury risks were in agreement with real-world injury incidence, the estimated abdominal injury risks were too low and needs further investigation. One of the reasons could be the use of a simplified vehicle model with a rigid center console and dashboard which may have affected occupant kinematics. Another limitation of the study was that the Camry-MDB impact for various PDOF was carried out by changing x- and y- velocities and keeping MDB's initial position the same for all the simulations rather than rotating it. This would have affected the intrusion profiles used in the study but the initial position was kept constant to reduce the number of variables between each simulation to improve comparisons between simulations. The intrusion profile was same for both the models in each case which allowed for relative differences to be studied within cases simulated.

CONCLUSIONS

This study employed a DOE approach with an FSVM incorporating intrusion to simulate and estimate injury risk for small females and average males in multiple far-side crash events. The injury risks increased with an increase in lateral ΔV . The average male had a higher risk of injury than a small female in all the body regions except the abdomen. The differences in injury risks between the male and female models were statistically significant. The effect of occupant size/sex on injury risk was highlighted by significant differences in overall injury risk for the small female vs. average male HBMs. Differences observed in the estimated injury risks suggest that occupant size/sex should be taken into consideration in safety system design.

ACKNOWLEDGEMENTS

This work was funded by the United States Council for Automotive Research (USCAR) under grant ID: 21-2262-USC. All simulations were run on the DEAC cluster at Wake Forest University with support from Stevens Cody and Adam Carlson.

DISCLOSURE STATEMENT

F. Scott Gayzik and Matthew Davis are members and Ashley A. Weaver is a consultant of Elemance, LLC., which distributes academic and commercial licenses for the use of GHBMCM-owned computational human body models.

REFERENCES

- [1] H. C. Gabler, K. Digges, B. N. Fildes, and L. Sparke, "Side impact injury risk for belted far side passenger vehicle occupants," *SAE transactions*, pp. 34-42, 2005.
- [2] B. Pipkorn *et al.*, "Occupant protection in far-side impacts," in *Proceedings of IRCOBI conference*, 2018, vol. 46, pp. 125-127.
- [3] M. W. J. Arun, S. Umale, J. R. Humm, N. Yoganandan, P. Hadagali, and F. A. Pintar, "Evaluation of kinematics and injuries to restrained occupants in far-side crashes using full-scale vehicle and human body models," *Traffic Injury Prevention*, vol. 17, no. sup1, pp. 116-123, 2016/09/12 2016, doi: 10.1080/15389588.2016.1197394.
- [4] K. Digges and D. Dalmotas, "Injuries to restrained occupants in far-side crashes," SAE Technical Paper, 2001.
- [5] Y. Kitagawa, S. Hayashi, K. Yamada, and M. Gotoh, "Occupant kinematics in simulated autonomous driving vehicle collisions: influence of seating position, direction and angle," SAE Technical Paper, 2017.
- [6] F. A. Pintar *et al.*, "Comparison of PMHS, WorldSID, and THOR-NT responses in simulated far side impact," *Stapp car crash journal*, vol. 51, p. 313, 2007.
- [7] R. Kent, J. Forman, D. Lessley, K. Arbogast, and K. Higuchi, "A parametric study of far-side restraint mechanics," in *Proc. Conference on the Enhanced Safety of Vehicles Paper*, 2013, no. 13-0381.
- [8] J. Broos and R. Meijer, "Simulation Method for Whiplash Injury Prediction Using an Active Human Model," in *Proceedings of the IRCOBI Conference*, 2016.

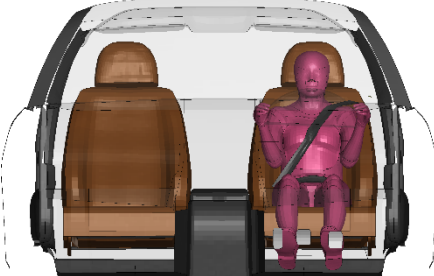

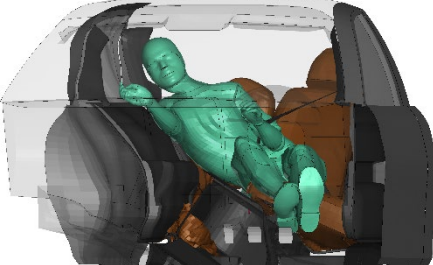
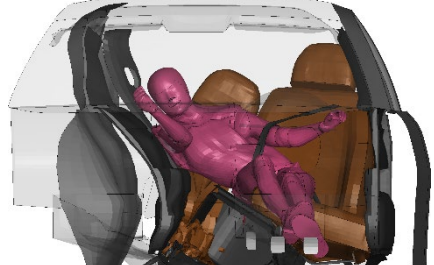
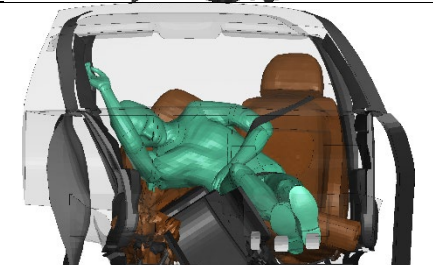

- [9] T. Ando, Y. Kitagawa, and A. Eggers, "Influence of Posture Adjustment Methods for Human Body Models on Injury Prediction," *Accident Reconstruction Journal*, vol. 30, no. 2, 2020.
- [10] W. B. Decker, D. A. Jones, K. Devane, M. L. Davis, J. P. Patalak, and F. S. Gayzik, "Simulation-based assessment of injury risk for an average male motorsport driver," *Traffic Inj Prev*, vol. 21, no. sup1, pp. S72-S77, Oct 12 2020, doi: 10.1080/15389588.2020.1802021.
- [11] W. B. Decker *et al.*, "Effect of body size and enhanced helmet systems on risk for motorsport drivers," *Traffic Injury Prevention*, vol. 22, no. sup1, pp. S49-S55, 2021/10/19 2021, doi: 10.1080/15389588.2021.1977802.
- [12] S. Kuppa, "Injury criteria for side impact dummies," *Washington, DC: National Transportation Biomechanics Research Center, National Highway Safety Administration, US DOT*, vol. 67, 2004.
- [13] H. J. Mertz, P. Prasad, and G. Nusholtz, "Head injury risk assessment for forehead impacts," *SAE transactions*, pp. 26-46, 1996.
- [14] P. Prasad and H. J. Mertz, "The position of the United States delegation to the ISO Working Group 6 on the use of HIC in the automotive environment," *SAE transactions*, pp. 106-116, 1985.
- [15] E. G. Takhounts, M. J. Craig, K. Moorhouse, J. McFadden, and V. Hasija, "Development of brain injury criteria (BrIC)," *Stapp car crash journal*, vol. 57, p. 243, 2013.
- [16] T. R. Laituri, S. Henry, K. Pline, G. Li, M. Frankstein, and P. Weerappuli, "New risk curves for NHTSA's brain injury criterion (BrIC): derivations and assessments," SAE Technical Paper, 2016.
- [17] F. Bandak *et al.*, "Development of improved injury criteria for the assessment of advanced automotive restraint systems: II," 1999.
- [18] K. Devane *et al.*, "Comparisons of head injury risk prediction methods to field data in far-side impacts," *Traffic Injury Prevention*, pp. 1-3, 2022, doi: 10.1080/15389588.2022.2124809.
- [19] Z. S. Hostetler *et al.*, "Injury risk curves in far-side lateral motor vehicle crashes by AIS level, body region and injury code," *Traffic Injury Prevention*, vol. 21, no. sup1, pp. S112-S117, 2020/10/12 2020, doi: 10.1080/15389588.2021.1880006.

APPENDIX A

Table A1. Results of statistical tests used for comparing model estimated injury risks

Injury Risk	Metrics Used	Linear Regression Parameters			Wilcoxon signed-rank p-value
		R ²	slope	intercept	
Head AIS2+ Injury Risk (NHTSA Curves)	HIC	0.57	0.54	0.42	0.000
Head AIS3+ Injury Risk (NHTSA Curves)	HIC	0.42	0.40	0.95	0.000
Head AIS2+ Injury Risk (Prasad and Mertz 1985)	HIC	0.58	0.60	0.14	0.000
Head AIS3+ Injury Risk (Prasad and Mertz 1985)	HIC	0.42	0.45	1.09	0.000
Head AIS2+ Injury Risk (Takhounts et al. 2013)	BrIC	0.95	1.06	-10.61	0.000
Head AIS3+ Injury Risk (Takhounts et al. 2013)	BrIC	0.79	0.74	3.34	0.000
Head AIS2+ Injury Risk (Laituri et al. 2016)	BrIC	0.61	0.27	1.29	0.000
Head AIS3+ Injury Risk (Laituri et al. 2016)	BrIC	0.62	0.24	0.31	0.000
Chest AIS2+ Injury Risk	CTI	0.88	0.85	10.89	0.774
Chest AIS3+ Injury Risk	Chest Deflection	0.01	0.02	0.95	0.000
Abdomen AIS3+ Injury Risk	Abdominal Force	0.84	0.72	0.16	0.656
Pelvis AIS3+ Injury Risk	Pubis Force	0.55	0.85	5.61	0.048
Overall AIS3+ Injury Risk	-	0.49	0.49	1.96	0.000

Table A2. Simulation snapshot for both models at various time

Time (ms)	M50-OS+B	F05-OS+B
0	 A top-down view of a car interior showing a green crash test dummy seated in the driver's seat, buckled up with a seatbelt. The car's body is shown in a semi-transparent grey.	 A top-down view of a car interior showing a pink crash test dummy seated in the driver's seat, buckled up with a seatbelt. The car's body is shown in a semi-transparent grey.
50	 A side view of the car interior showing the green crash test dummy leaning back and slightly to the left. The car's body is shown in a semi-transparent grey.	 A side view of the car interior showing the pink crash test dummy leaning back and slightly to the right. The car's body is shown in a semi-transparent grey.
75	 A side view of the car interior showing the green crash test dummy leaning further back and to the left. The car's body is shown in a semi-transparent grey.	 A side view of the car interior showing the pink crash test dummy leaning further back and to the right. The car's body is shown in a semi-transparent grey.
100	 A side view of the car interior showing the green crash test dummy leaning significantly back and to the left. The car's body is shown in a semi-transparent grey.	 A side view of the car interior showing the pink crash test dummy leaning significantly back and to the right. The car's body is shown in a semi-transparent grey.
150	 A side view of the car interior showing the green crash test dummy leaning almost horizontally back and to the left. The car's body is shown in a semi-transparent grey.	 A side view of the car interior showing the pink crash test dummy leaning almost horizontally back and to the right. The car's body is shown in a semi-transparent grey.